DISTRIBUTION AND CHARACTERIZATION OF IRON IN IMPLANTED SILICON CARBIDE

CONF-911202--14

DE92 005126

J. BENTLEY, L. J. ROMANA, L. L. HORTON, and C. J. McHARGUE*
Metals and Ceramics Division, Oak Ridge National Laboratory, P. O. Box 2008, Oak Ridge, TN 37831-6376.
*The University of Tennessee, Knoxville, TN 37993.

ABSTRACT

Analytical electron microscopy (AEM) and Rutherford backscattering spectroscopy-ion channeling (RBS-C) have been used to characterize single crystal α-silicon carbide implanted at room temperature with 160 keV ^{57}Fe ions to fluences of 1, 3, and 6×10^{16} ions/cm^2. Best correlations among AEM, RBS, and TRIM calculations were obtained assuming a density of the amorphized implanted regions equal to that of crystalline SiC. No iron-rich precipitates or clusters were detected by AEM. Inspection of the electron energy loss fine structure for iron in the implanted specimens suggests that the iron is not metallically-bonded, supporting conclusions from earlier conversion electron Mössbauer spectroscopy (CEMS) studies. In-situ annealing surprisingly resulted in crystallization at 600°C with some redistribution of the implanted iron.

The submitted manuscript has been authored by a contractor of the U.S. Government under contract No. DE-AC05-84OR21400. Accordingly, the U.S. Government retains a nonexclusive, royalty-free license to publish or reproduce the published form of this contribution, or allow others to do so, for U.S. Government purposes.

INTRODUCTION

Effective use of ion implantation for the surface modification of ceramics requires that an understanding be developed of the fundamental materials science of the interactions of the implanted species with the host. Whereas extensive work has been done to characterize the nature (charge state, bonding, etc.) of the implanted species for Al_2O_3, less work has been performed on ion-implanted silicon carbide (see, for example, the review by White et al., ref. [1]). Silicon carbide is easily amorphized; the critical damage energy density for amorphization of α-SiC at room temperature is between 0.02 and 0.05 keV/atom [2-5]. Conversion electron Mössbauer spectroscopy (CEMS) of ^{57}Fe implanted into single crystals of α-SiC suggested a distribution of the iron among several sites with slightly different local symmetries and the presence of covalent iron compounds or low spin iron complexes with covalent bonding [6]. One purpose of the current study was to further characterize the same specimens used for the CEMS examination with analytical electron microscopy (AEM) and Rutherford backscattering spectroscopy (RBS) to obtain additional information about the implanted iron.

EXPERIMENTAL PROCEDURE

Polished single crystal α-SiC platelets (Carborundum Company, Niagara Falls, NY) of predominately the 6H polytype with the broad face parallel to the basal (0001) plane were implanted at room temperature with 160 keV ^{57}Fe to fluences of 1, 3, and 6×10^{16} ions/cm^2 and analyzed by Rutherford backscattering-ion channeling (RBS-C) with 2.3 MeV He^+ ions at the ORNL Surface Modification and Characterization Facility.

Analytical electron microscopy was performed at 100 kV with a Philips EM400T equipped with a field emission gun, a 6585 scanning transmission electron microscopy (STEM) unit, an EDAX 9100/70 energy dispersive X-ray spectrometer (EDS), and a Gatan 666 parallel-detection electron energy loss spectrometer (PEELS). X-ray microanalysis line-scans were performed in the STEM mode with a probe of $\leq$3 nm diameter, ~1 nA probe current, and X-ray count rates of 2,000 to 3,000 counts/s. An analogue scan was employed; each data point in the EDS profiles was obtained in 4 s, during which time the probe advanced 7.4 nm. Since this distance is greater than the probe size and the expected beam broadening, it defines the spatial resolution. The precision of the peak composition is limited to $\leq$3% by counting statistics. Integrated X-ray intensities, $I_{Fe,Si}$, were converted to composition $C_{Fe,Si}$ (atomic %) from the relationship: $C_{Fe}/C_{Si} = k_{FeSi}\, I_{Fe}/I_{Si}$, where $k_{FeSi} = 0.708$, as calculated with an updated version of the computer code (NEDQNT2) based on the standardless approach of Zaluzec [7].

J. Bentley

DISTRIBUTION OF THIS DOCUMENT IS UNLIMITED

DISCLAIMER

This report was prepared as an account of work sponsored by an agency of the United States Government. Neither the United States Government nor any agency thereof, nor any of their employees, makes any warranty, express or implied, or assumes any legal liability or responsibility for the accuracy, completeness, or usefulness of any information, apparatus, product, or process disclosed, or represents that its use would not infringe privately owned rights. Reference herein to any specific commercial product, process, or service by trade name, trademark, manufacturer, or otherwise does not necessarily constitute or imply its endorsement, recommendation, or favoring by the United States Government or any agency thereof. The views and opinions of authors expressed herein do not necessarily state or reflect those of the United States Government or any agency thereof.

Specimens were prepared in both cross-section and plan-view geometries. For plan view specimens, prior to conventional backthinning, ~80 nm of material was removed from the implanted surface by ion milling, the conditions (100 s, 3 keV, 20° milling angle) being determined from trial runs in which half of the specimen surface was masked. After sectioning, the implanted surface was coated with salt to allow easy removal of material deposited during the back-thinning operation of the ion mill [8].

ANALYTICAL ELECTRON MICROSCOPY RESULTS

A cross-sectional micrograph of the specimen implanted with 6×10^{16} ions/cm^2 is shown in Fig. 1. The implanted region extending to 195 nm from the surface is amorphous, as confirmed by convergent beam electron diffraction (CBED) patterns, and contains iron at levels easily detectable by EDS. The 1.5 nm lattice fringes of the edge-on 6H basal planes in the substrate provide an unambiguous depth calibration scale. The transition layer at the end of the ion range exhibits the expected strain contrast.

The depth profile of the implanted iron was measured by EDS line scans perpendicular to the implant surface. The results of three of these scans are shown in Fig. 2 and summarized in Table I. Assuming a density for amorphous SiC equal to that of its crystalline forms, the integrated iron profile is the expected 6.0×10^{16} ions/cm^2. McHargue et al. [9] showed that SiC swelled by 20% when amorphized by Cr-implantation, but if this lower SiC density is assumed, the integrated iron profile is reduced to 4.8×10^{15} ions/cm^2.

In order to better search for evidence of iron clustering, as observed for Al_2O_3 implanted with 1×10^{17} Fe/cm^2 [10], a plan-view specimen sectioned to near the peak iron deposition was examined. EDS confirmed that this region was obtained. Figure 3 shows a through-focus-series at high magnification. Iron-rich precipitates or clusters with diameters >2 nm would have been clearly visible, but no precipitates were observed.

Information about the bonding of the iron was obtained from examination of the electron energy loss fine structure for the iron L_3 edge. Fig. 4 shows a comparison of the fine structure for this edge in spectra measured with PEELS for the plan-view Fe-implanted SiC specimen and for

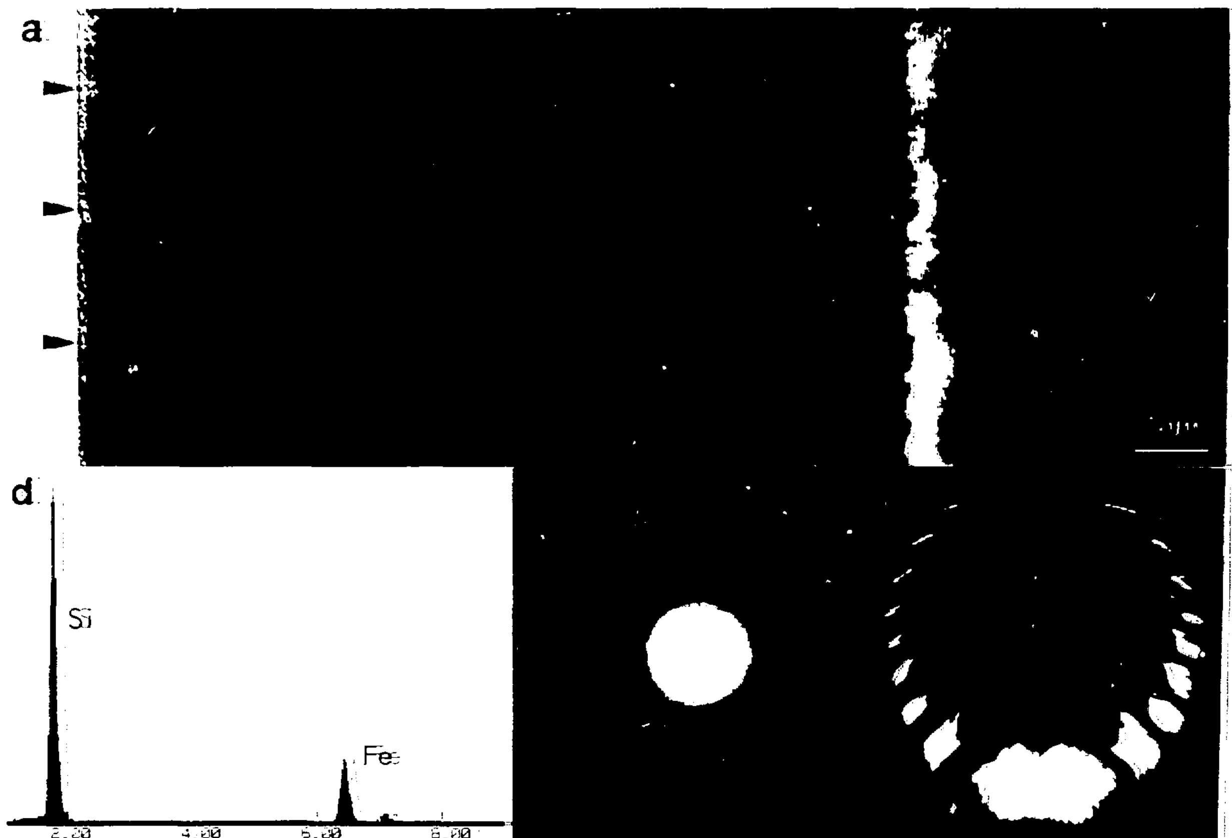

Fig. 1. (a) Micrograph of cross-sectioned SiC implanted with 6×10^{16} Fe ions/cm^2. (b,c) CBED patterns from the crystalline substrate and the amorphous implanted layer, respectively. (d) Energy-dispersive X-ray spectrum from the implanted region.

Table I: Comparison of AEM, RBS-C, and TRIM data for implanted iron and damage profiles.

Technique	Nominal Fluence (10^{16} /cm^2)	Assumed Density (g/cm^3)	Amorphized Depth (nm)	Iron Peak (nm)	FWHM (nm)	Peak Fe/SiC (mol %)	Integrated Iron Profile (10^{16} /cm^2)
AEM	6	3.2	195	85	80	16	6.0
		2.6					4.8
RBS-C	3	3.2	200	75	80	7	2.8
		2.6	250	90	110	7	2.8
TRIM	6	3.2	150	88	64	20	
		2.6	200	110	80	20	

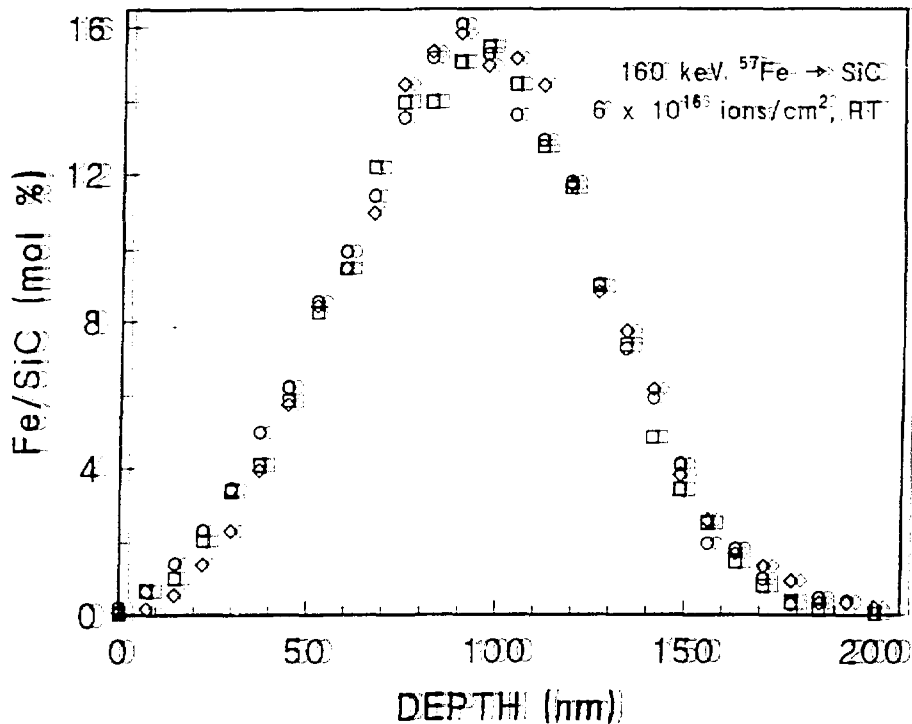

Fig. 2. Fe depth profile measured by EDS in SiC implanted with 6×10^{16} Fe ions/cm^2. Data shown are from three separate scans across the implanted region of the specimen.

Fig. 3. High magnification images of a plan-view specimen sectioned to allow examination of region with the peak iron concentration. Through-focus series in steps of 80 nm; no precipitates are observed (observation limit ~2 nm).

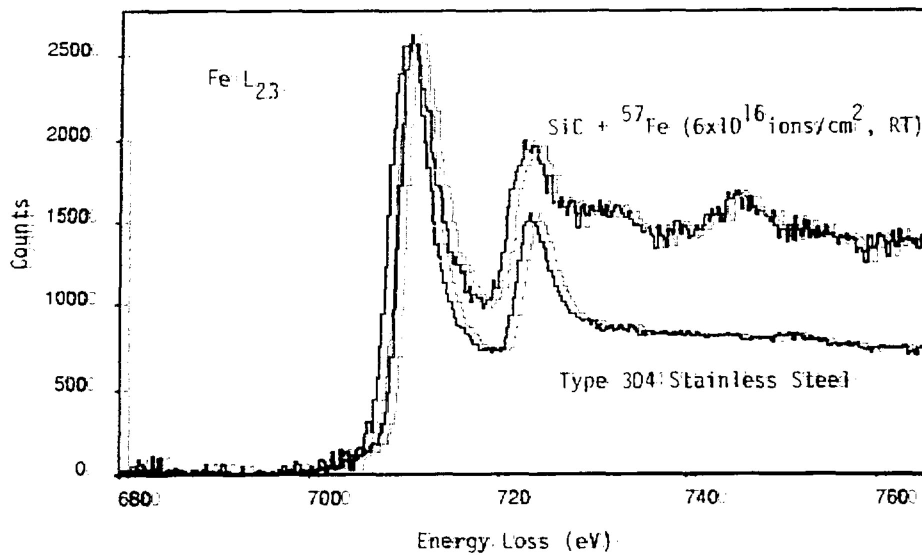

Fig. 4. PEELS fine structure of the background-subtracted iron L_{23} edge for Fe-implanted SiC and type 304 stainless steel.

metallically-bonded-iron in type 304 stainless steel. The "white lines" at ~711 and ~724 eV in the spectrum from Fe-implanted SiC are much broader and of lower intensity relative to the contribution from the continuum states than those in the spectrum from the stainless steel. White lines arise from transitions to unfilled, bound states just above the Fermi level; the detailed near-edge fine structure is thus a sensitive indicator of chemical bonding. The strength of the signal representing transitions to continuum states (the region above ~735 eV) provides a good measure of the quantity of the iron analyzed. The results suggest that the iron in the SiC is not primarily metallically-bonded and support the conclusion of the earlier CEMS data that the iron is in covalently bonded sites [6].

RUTHERFORD BACKSCATTERING-CHANNELING RESULTS

Channeling RBS experiments demonstrated that the implanted specimens were amorphous even at the lowest fluence. Typical spectra are shown in Fig. 5 for the specimen implanted to 3×10^{16} ions/cm^2 and are plotted assuming a density for amorphous SiC equal to that of crystalline

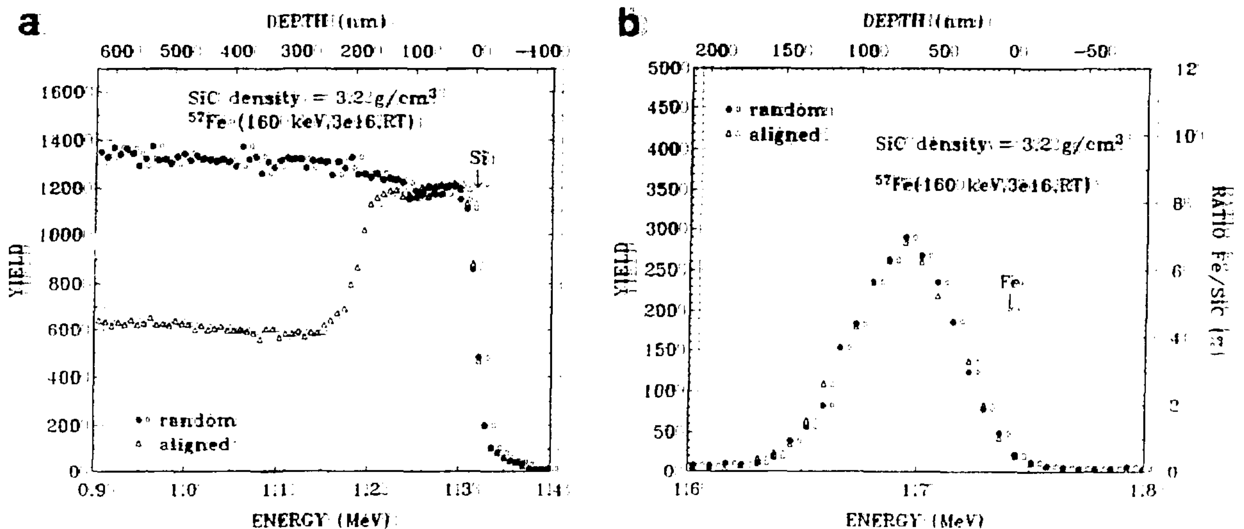

Fig. 5. RBS spectra for SiC implanted with 3×10^{16} Fe ions/cm^2 assuming the density of the amorphous region is equal to that of crystalline SiC. (a) Silicon (b) Iron.

material. The damage and implanted iron profiles for this specimen were also calculated with a 20% lower density for amorphous SiC. The profile parameters are summarized in Table I.

COMPARISON OF AEM, RBS, AND TRIM CALCULATIONS

Table I summarizes TRIM [11] calculations for the two densities of SiC, 3.2 g/cm^3 (crystalline) and 2.6 g/cm^3 (amorphous), that were discussed above relative to the interpretation of the RBS and AEM data. The values listed for the amorphized depth calculated with TRIM correspond to the end of the deposited ion and collision profiles. Comparisons of the TRIM calculations with the RBS and AEM data are complex. No firm conclusions can be drawn from a comparison of the TRIM and RBS ion range values; the higher density values disagree by 15% and the values for the lower density disagree by 18%. However, good agreement for the ion range is seen between the AEM results and TRIM calculations for the higher density. The FWHM value for the RBS experiment, assuming a crystalline density, also agrees with the 80 nm value measured with AEM. The integrated iron profile calculated from the AEM data agrees with the experimental fluence only for the higher density.

IN-SITU ANNEALING

In an attempt to promote the deposited iron to change its form or distribution, a cross-sectioned AEM specimen was annealed in-situ. No changes, such as clustering of the Fe, were observed after annealing at up to 550°C. Surprisingly, at 600°C the amorphous layer began to crystallize. The transformation began in the middle of the layer at the foil edge and proceeded in a direction parallel to the original surface (see Fig. 6). After a few minutes the heater current was turned off, quenching the specimen. The crystallized material was heavily defected and twinned (cubic) silicon carbide with the growth direction along $<111>_\beta$. Similar in-situ annealing of Cr-implanted polycrystalline SiC by Sklad et al. [12] achieved only slight epitactic regrowth from the substrate at up to 1100°C. Bohn et al. showed that annealing at 1500°C was necessary for complete epitactic regrowth in Cr-implanted SiC [13].

The iron profile in the crystallized material was measured by EDS line scans (Fig. 7). Some redistribution of the Fe is noticeable in the lowered and broadened profile. The local variations in the Fe signal may be due to precipitation of the iron, but the high defect density and specimen thickness preclude reaching any firm conclusions from the image. The possibility of rejection of the iron to the foil surfaces also has to be considered.

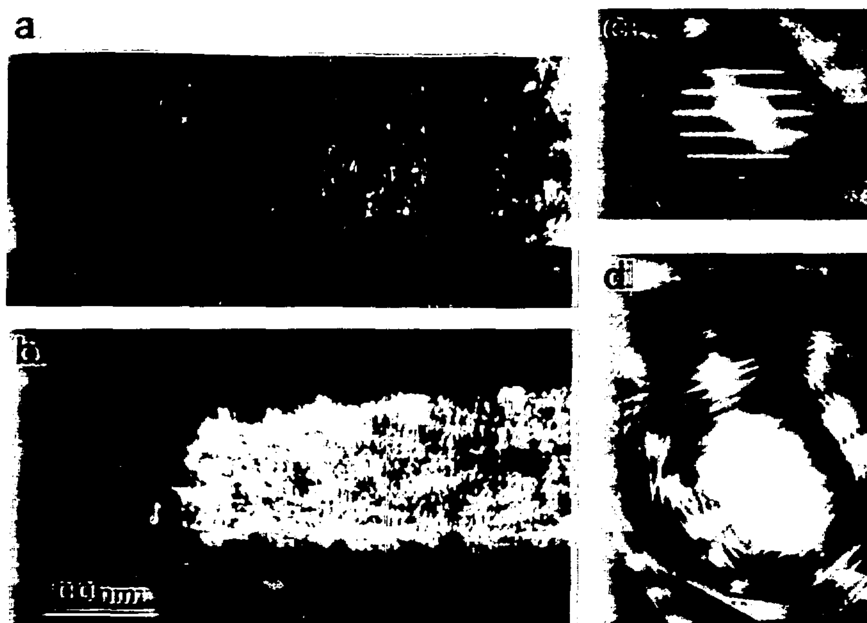

Fig. 6. (a) Bright-field and (b) dark-field images of crystallized region in cross-sectioned SiC annealed in-situ at 600°C. (c,d) Diffraction patterns showing growth along approximately $<111>_\beta$, normal to $[0001]_{6H}$ substrate.

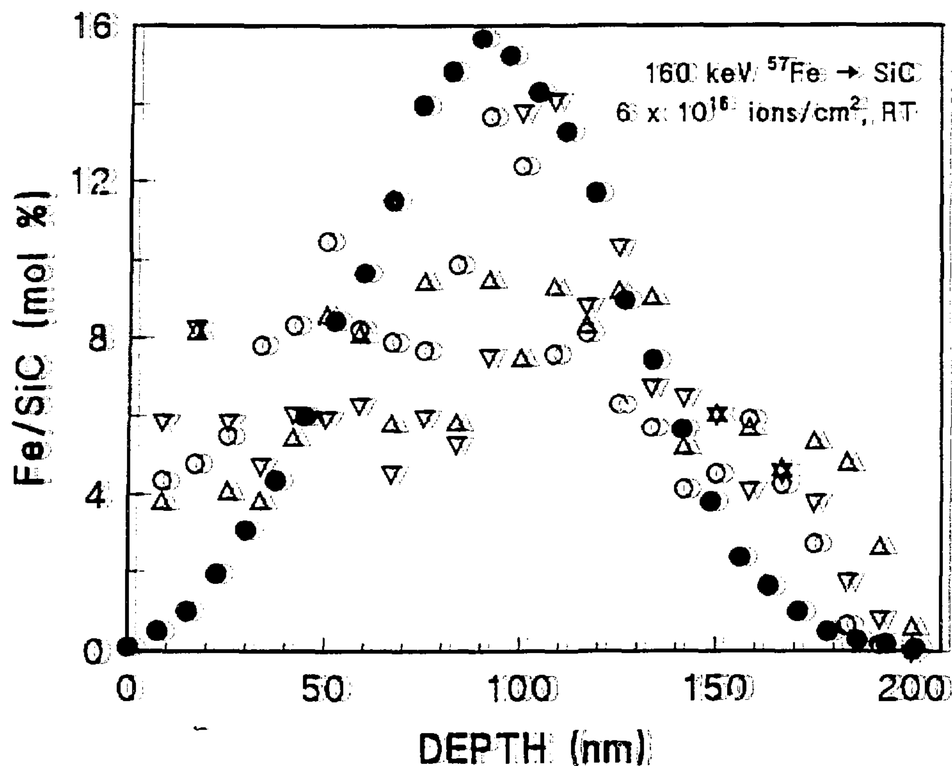

Fig. 7. Fe depth profiles measured by EDS in implanted SiC. Solid symbols: as-implanted. Open symbols: after crystallization by annealing in-situ at 600°C (3 data sets).

ACKNOWLEDGEMENTS

The authors thank Drs. N. D. Evans, P. S. Sklad, P. Thevenard, and J. Pawel for helpful discussions, and A. M. Williams and A. T. Fisher for electron microscopy specimen preparation. Research sponsored by the Division of Materials Sciences, U.S. Department of Energy under contract DE-AC05-84OR21400 with Martin Marietta Energy Systems, Inc.

REFERENCES

1. C.W. White, C.J. McHargue, P.S. Sklad, L.A. Boatner, and G.C. Farlow, Mat. Sci. Reports 4, 41 (1989).
2. J.M. Williams, C.J. McHargue, and B.R. Appleton, Nucl. Instr. and Meth. **209/210**, 317 (1983).
3. P.J. Burnett and T.F. Page, J. Mater. Sci. **19**, 845 (1984).
4. J.A. Spitznagel, S. Wood, W.J. Choyke, N.J. Doyle, J. Bradshaw, and S.J. Fishman, Nucl. Instr. and Meth. **B16**, 237 (1986).
5. J.A. Edmond, R.F. Davis, S.P. Withrow, and K.L. More, J. Mater. Res. **3**, 321 (1988).
6. C.J. McHargue, A. Perez, and J.C. McCallum, Nucl. Inst. and Meth. **B59/60**, 1362-5 (1991).
7. N. J. Zaluzec, Ch. 4 in Introduction to Analytical Electron Microscopy, eds. J.J. Hren, J.I. Goldstein, and D.C. Joy (Plenum Press, New York, 1979).
8. A.T. Fisher and P. Angelini, in Proc. 43rd Ann. Meet. Electron Microscopy Soc. Amer., ed. G.W. Bailey (San Francisco Press, San Francisco, CA, 1985) pp. 182-3.
9. C.J. McHargue and J.M. Williams, in Metastable Materials Formation by Ion Implantation (Mater. Res. Soc. Symp. Proc. 7), eds. S.T. Picraux and W.J. Choyke (North Holland, New York, 1982) p. 303-9.
10. P.S. Sklad, J.C. McCallum, S.J. Pennycook, C.J. McHargue, C.W. White, and A. Perez, in Characterization of the Structure and Chemistry of Defects in Materials, eds. B.C. Larson, M. Rühle, and D.N. Seidman (Mater. Res. Soc. Proc. 138, Pittsburgh, PA, 1989) pp. 119-124.
11. J.P. Biersack and L.G. Haggmark, Nucl. Instr. and Meth. **174**, 257 (1980).
12. P.S. Sklad, P. Angelini, C.J. McHargue, and J.M. Williams, in Proc. 42nd Ann. Meet. Electron Microscopy Soc. Amer., ed. G. W. Bailey (San Francisco Press, San Francisco, CA, 1984) pp. 416-7.
13. H.G. Bohn, J.M. Williams, C.J. McHargue, and G.M. Begun, J. Mater. Res. **2**, 107 (1987).

J. Bentley
6
6